

## Introduction

Seismic imaging and inversion relies on scattered waves to locate and infer property contrasts in the Earth's subsurface. To target the reconstruction of only the desired scattered waves by seismic interferometry (e.g., Wapenaar and Fokkema, 2006), here I present a perturbation-based formulation (Vasconcelos and Snieder, 2008) that retrieves the causal scattered waves that propagate between two receivers as if one acts as a pseudo-source.

Other formulations of interferometry (e.g., Wapenaar et al., 2006; Schuster and Zhou, 2006) retrieve, apart from the scattered waves, the full response between receivers. Mehta et al. (2007) proposed the use of wavefield separation in interferometry to target desired arrivals. In this paper I connect some of their findings to the perturbation-based representation. In particular, Mehta et al. (2007) demonstrated the potential of using wavefield separation in the interferometry of OBC data. In the same context as Mehta et al., the perturbation-based approach discussed here can be used to extract multiple-free scattered waves in OBC experiments. This is demonstrated with two synthetic data examples.

In seismic migration, a common imaging condition consists of cross-correlating data-derived scattered waves with a modeled reference field at depth (Claerbout, 1985). This imaging condition serves as the basis for describing the subsurface reflectivity at depth (Sava and Fomel, 2003), but this can only be accomplished if the imaging scheme is capable of properly reconstructing scattered-wave amplitudes. The exact form of the perturbation-based theorem presented here can possibly provide contributions for amplitude-preserving migration schemes, as well as for migrating multiply-scattered waves.

### Perturbation-based representations

*Representation theorems in perturbed media.* In arbitrarily complex perturbed acoustic media, the wavefield perturbations  $G_S$  between two observation points  $\mathbf{r}_A$  and  $\mathbf{r}_B$  can be retrieved according to the following frequency-domain representation theorem (Vasconcelos and Snieder, 2008a):

$$G_S(\mathbf{r}_B, \mathbf{r}_A) = \oint_{\partial\mathbb{V}} \frac{1}{i\omega\rho} [G_S(\mathbf{r}, \mathbf{r}_A)\nabla G_0^*(\mathbf{r}, \mathbf{r}_B) + G_0^*(\mathbf{r}, \mathbf{r}_B)\nabla G_S(\mathbf{r}, \mathbf{r}_A)] \cdot d\mathbf{S} + \int_{\mathbb{V}} i\omega(\kappa_0 - \kappa)G(\mathbf{r}, \mathbf{r}_A)G_0^*(\mathbf{r}, \mathbf{r}_B)dV ; \quad (1)$$

where  $G_0$  are unperturbed waves,  $G = G_0 + G_S$  are perturbed waves,  $\omega$  is frequency,  $\rho$  is the spatially-varying density, and  $\kappa$  and  $\kappa_0$  are the perturbed and unperturbed compressibilities, respectively. The source position  $\mathbf{r}$  is integrated over the closed surface  $\partial\mathbb{V}$  (first integral) and also over the volume  $\mathbb{V}$  (second integral).  $G_0^*$  is the complex-conjugate of  $G_0$ , and translates into a cross-correlation in the time-domain. Although not shown here, these results have been generalized to many perturbed physical systems (e.g., attenuative acoustic, elastic and electromagnetic waves, diffusive transport).

*Reconstructing scattered waves with interferometry.* The purpose of interferometry is to reconstruct the impulse response between two points  $\mathbf{r}_A$  and  $\mathbf{r}_B$  with no knowledge of model parameters. Although equation 1 retrieves  $G_S(\mathbf{r}_B, \mathbf{r}_A)$ , the evaluation of the volume integral requires knowledge of the medium perturbations inside  $\mathbb{V}$ . However, when the receivers lie between surface sources and the scatterers in a perturbation volume  $\mathbb{P}$  (Figure 1a), the volume integral in equation 1 can be ignored (Vasconcelos and Snieder, 2008). Thus, equation 1 can be approximated to

$$G_S(\mathbf{r}_B, \mathbf{r}_A) \approx \int_{\mathbf{r} \in \partial\mathbb{V}_1} \frac{1}{i\omega\rho} [G_S(\mathbf{r}, \mathbf{r}_A)\nabla G_0^*(\mathbf{r}, \mathbf{r}_B) + G_0^*(\mathbf{r}, \mathbf{r}_B)\nabla G_S(\mathbf{r}, \mathbf{r}_A)] \cdot d\mathbf{S}; \quad (2)$$

where  $\partial\mathbb{V}_1$  is a portion of  $\partial\mathbb{V}$  for which the contribution of the  $G_0 G_0^*$ -term of the volume integral in equation 1 vanishes, i.e., when receivers lie between the sources and the scatterers (Figure 1a). Equation 2 is suitable for interferometry because unlike equation 1 it does not require prior knowledge of model parameters. When only pressure measurements are available, equation 2 can be recast as

$$G_S(\mathbf{r}_B, \mathbf{r}_A) \approx \int_{\mathbf{r} \in \partial\mathbb{V}_1} \frac{2}{\rho c} G_S(\mathbf{r}, \mathbf{r}_A) G_0^*(\mathbf{r}, \mathbf{r}_B) dS ; \quad (3)$$

by applying  $\nabla G \cdot d\mathbf{S} = i(\omega/c)GdS$ . This approximation assumes that  $\partial\mathbb{V}$  is a sphere of infinite radius and that all scattered waves are outgoing at  $\partial\mathbb{V}$  (Wapenaar and Fokkema, 2006). The majority of implementations of seismic interferometry uses a formulation similar to equation 3. Indeed, equation 3 is the only feasible way to perform interferometry when only pressure measurements are available (e.g., Wapenaar and Fokkema, 2006). However, as shown below for the case of dual-field ocean-bottom records, equation 2 is more appropriate for interferometry.

*Connection to seismic imaging.* An imaging condition that is commonly used in seismic migration is given by (e.g., Claerbout, 1985)

$$\mathcal{I}(\mathbf{r}_A) = \sum_{\text{all } \omega} G_S(\mathbf{r}_A, \mathbf{r}_A) = \sum_{\text{all } \omega} \left[ \int_{\partial\mathbb{V}} G_S(\mathbf{r}, \mathbf{r}_A) G_0^*(\mathbf{r}, \mathbf{r}_A) dS \right] ; \quad (4)$$

where  $\mathcal{I}$  is the seismic image at  $\mathbf{r}_A$  and summation is carried out over all frequencies  $\omega$ . In the case of shot-profile migration, for example, the integral in equation 4 represents a summation over shots  $\mathbf{r}$ . In order to generate a complete image of the volume  $\mathbb{V}$ , equation 4 must be evaluated repeatedly at all points  $\mathbf{r}_A$  within the volume. In typical seismic experiments  $G_S$  is part of the acquired data for varying  $\mathbf{r}$  (e.g., sources) and  $\mathbf{r}_A$  on the surface (i.e., on  $\partial\mathbb{V}$ ). Inside  $\mathbb{V}$ , the response  $G_S(\mathbf{r}, \mathbf{r}_A)$  is typically modeled from the acquired data, e.g., by wavefield extrapolation. Note that the integrand in equation 4 is the same as the integrand in the expression for perturbation-based interferometry in equation 3, apart from the  $2/\rho c$  scaling. In equation 4, the image is defined as the zero-offset scattered-wave response summed over  $\omega$ , which in the time-domain is  $G_S(\mathbf{r}_A, \mathbf{r}_A, t = 0)$ . For equations 4, 3 and 1, it follows that an exact expression for  $G_S(\mathbf{r}_A, \mathbf{r}_A, t = 0)$ , i.e., for the image is given by

$$\begin{aligned} \mathcal{I}'(\mathbf{r}_A) = \sum_{\text{all } \omega} G_S(\mathbf{r}_A, \mathbf{r}_A) &= \sum_{\text{all } \omega} \left[ \oint_{\partial\mathbb{V}} \frac{1}{i\omega\rho} [G_S(\mathbf{r}, \mathbf{r}_A) \nabla G_0^*(\mathbf{r}, \mathbf{r}_B) + G_0^*(\mathbf{r}, \mathbf{r}_B) \nabla G_S(\mathbf{r}, \mathbf{r}_A)] \cdot d\mathbf{S} \right] \\ &+ \sum_{\text{all } \omega} \left[ \int_{\mathbb{V}} i\omega(\kappa_0 - \kappa) G(\mathbf{r}, \mathbf{r}_A) G_0^*(\mathbf{r}, \mathbf{r}_B) dV \right] . \end{aligned} \quad (5)$$

When only pressure records are available, the surface integral in equation 5 can be replaced by that in equation 3<sup>1</sup>. Note that in equation 5,  $G_S$  is the full scattered wavefield. This justifies, for example, the fact that reverse-time migration images multiply-reflected waves when the velocity model contains abrupt changes in the velocity model. In principle, including the volume integral of equation 5 can provide an extra correction for amplitudes and artifacts for any type of seismic migration method.

### Acoustic examples of interferometry: point-scatterers and OBC

For these synthetic examples, I use the models displayed in Figures 1b and 1c. The first model (Figure 1b) consists of three point scatterers embedded in a homogeneous acoustic medium of wavespeed  $c = 1.5$  km/s. This model is used to illustrate the effect of the far-field radiation approximation used to derive equation 3. A second model (Figure 1c), containing both point-scatterers and flat layer-like structures, is used to address the application of equations 2 and 3 for processing P-wave OBC data. When modeling data for either model, a line of sources is placed horizontally at  $z = 0.05$  km with source spacing of 2 m.

For the point-scatterer model (Figure 1b), the data are recorded at two receivers: one at (0.3, 0.2) and another at (0.7, 0.2). In this point-scatterer case, the receiver-gather data are modeled both with and without a free-surface at the top of the model. Figures 2a and 2b displays the integrands of equations 3 and 2, respectively, for the data modeled without the free-surface. The same integrands are portrayed in Figures 2c and 2d, but there the input data are generated with a free-surface. When the free-surface is absent, the integrands of both equations 3 and 2 (Figures 2a and 2b) yield practically the same result, apart from a difference between their

<sup>1</sup>In this case, the far-field radiation boundary condition applies (e.g., Wapenaar and Fokkema, 2006).

pulse shapes<sup>2</sup>. In the presence of the free-surface, the integrand of equation 3 (Figure 2c) is substantially different from that of equation 2 (Figure 2d), especially for times later than 0.6 s. Here, the data in presence of the free-surface contains both out- and in-going scattered waves at the integration surface  $\partial V_1$  (i.e., the source line in Figure 1c). Since equation 3 assumes that only out-going scattered waves are present, the results in Figures 2c and 2d are different. As we discuss below, the events that are canceled at times later than 0.6 s in Figure 2d are free-surface multiples associated to the scattered wavefield.

Perturbation-based interferometry as I present here can be applied to OBC data. Figures 3c and 3d show pseudo-shot gathers obtained by perturbation-based interferometry applied to the OBC data generated for the model in Figure 1c in the presence of a free-surface. The physical source response corresponding to the pseudo-shot gathers are shown in Figures 3a and 3b. Similarly to the point-scatterer examples in Figures 2c and 2d, the pseudo-shot gather produced by equation 3 (Figure 3d) shows many events at later times that are not present in the pseudo-shot generated with equation 2 in Figure 3c. Furthermore, by comparing Figures 3a and 3b with Figures 3c and 3d, we observe that equation 2 retrieves a pseudo-response without free-surface multiples (shown in Figure 3a); while data reconstructed with equation 3 contains all free-surface multiples. In the integrand of equation 2, the terms  $(G_S^A \nabla G_0^{B*})$  and  $(\nabla G_S^A G_0^{B*})$  always have opposite signs for free-surface multiples because the free-surface induces a polarity flip for  $G$  but not for  $\nabla G$ . This leads to the cancelation of multiples seen in Figures 2d and 3c. This property does not hold for interferometry of single wavefields (e.g., equation 3), as demonstrated in Figure 2c and 3d. Note that the approach I use here does not rely on the separation of up- and down-going fields (e.g., Mehta et al., 2008a). Mehta et al. (2008) use time gating and up/down separation to compute an integrand of the form  $(G^A + \nabla G^A)G_0^{B*}$ , which differs from that in the representation theorem in equation 2.

### Conclusion

Perturbation-based interferometry recovers only the causal scattered wavefield, desired for imaging purposes. The approach can be applied both for dual- or single-field data. This method is particularly advantageous for dual-field measurements, from which it can recover the response between receiver without free-surface multiples. This type of interferometry requires the prior separation of reference and scattered fields, which can be accomplished by different methods such as time-gating, Radon-type separation, or data-convolution methods (e.g., as in SRME). I illustrate the method with synthetic data examples, and in particular, demonstrate its applicability to OBC data. Here I also explicitly outline how the exact form of perturbation-based representation can lead to the imaging condition in seismic migration that cross-correlates downward-propagated scattered waves with a forward-modeled reference field. In this context, the exact form of the perturbation-based theorem can possibly aid in migrating multiples, as well as in providing corrections for migration amplitudes and artifacts.

### References

- [1] J.F. Claerbout. *Imaging the Earth's Interior*. Blackwell Publishing, 1985.
- [2] J. Gaiser and I. Vasconcelos. Elastic interferometry of OBC data – Theory and Examples. *EAGE Expanded Abstracts*, submitted, 2008.
- [3] K. Mehta, R. Snieder, R. Calvert and J. Sheiman. Improving the virtual source method by wavefield separation. *Geophysics*, V79–V86, 2007.
- [4] P. Sava and S. Fomel. Angle-domain common-image gathers by wavefield continuation methods. *Geophysics*, 68:1065-1074, 2003.
- [5] I. Vasconcelos and R. Snieder. Representation theorems and Green's function retrieval in perturbed acoustic media. *Phys. Rev. E*, submitted, 2008.
- [6] K. Wapenaar and J. Fokkema. *Geophysics*, 71:SI133–SI146, 2006.

---

<sup>2</sup>The pulse-shape difference between Figures 2a and 2b arises from the  $(i\omega)^{-1}$  factor present in the integrand in equation 2.

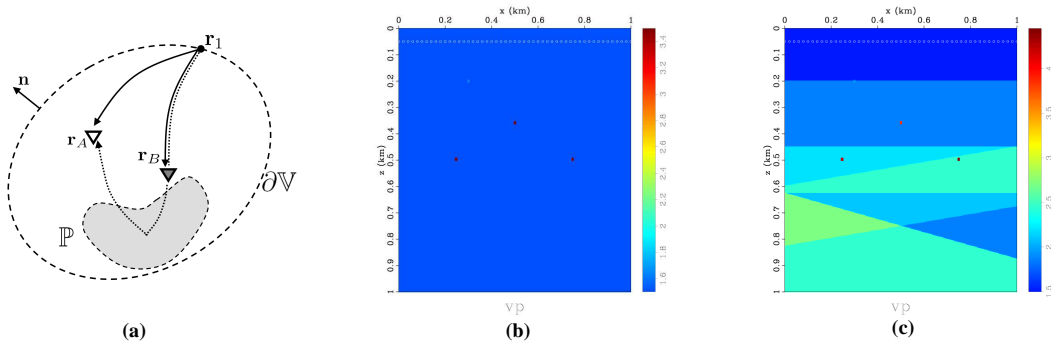


Figure 1: Models considered for perturbation-based interferometry. Panel (a) is a schematic representation of the class of models for which the approximation in equation 2 is valid. In (b) I show the model used for the point-scatterer examples in Figure 2. The velocity model in (c) is used in the OBC synthetic example (Figure 3). Both in (b) and in (c), the dotted line represents the physical source line, and the color-scale indicates the acoustic wavespeed in km/s.

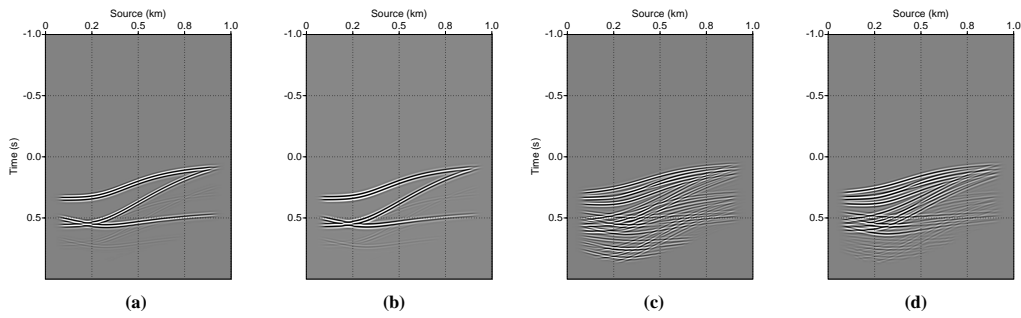


Figure 2: Cross-correlation gathers from a pair of receivers in the model in Figure 1b. The data input in (a) and (b) are modeled *without* a free-surface, whereas the input to (c) and (d) is modeled *with* a free-surface. The gathers in (a) and (c) are obtained using equation 3; while the gathers in (b) and (d) are computed according to equation 2. In this case,  $\mathbf{r}_A = (x = 0.7, z = 0.2)$  and  $\mathbf{r}_B = (0.3, 0.2)$ . Here,  $G_0$  consists of the superposition of direct waves and all water-bottom multiples;  $G_S$  is the scattered wavefield generated by the subsurface structure.

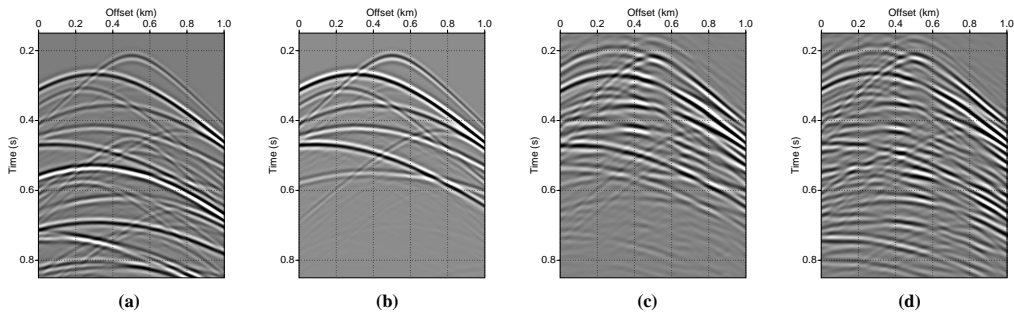


Figure 3: True responses and pseudo-shot gathers. The true scattered-wave response for a physical source at  $(0.3, 0.2)$  (see Figure 1c) is displayed in (a) modeled *with* a free-surface, and in (b), where it is modeled *without* a free-surface. Pseudo-shot gathers are shown in (c) and in (d) for a pseudo-source at  $\mathbf{r}_A = (0.3, 0.2)$ . The result in (c) is obtained with equation 2; while (d) results from applying equation 3. It is important to note that the input data *to both* (c) and (d) were modeled *with* a free-surface.